1 Description of tree species groups

Table S 1. Classification of samples from different tree species within the processed dataset (i.e. after outlier correction) into groups of tree species and respective total number of samples within the processed dataset, including samples from all needle age classes.

Tree species group	Tree species	n samples
ash	*Fraxinus excelsior*	10
beech	*Fagus sylvatica*	372
birch	*Betula pendula*	1
Douglas fir	*Pseudotsuga menziesii*	55
fir	*Abies alba*	162
	Abies borisii regis	3
hornbeam	*Carpinus betulus*	10
larch	*Larix decidua*	3
oak	*Quercus petraea*	133
	Quercus robur	101
	Quercus (mix: *Quercus petraea* and *Quercus robur*)	42
	Quercus cerris	4
	Quercus ilex	4
	Quercus frainetto	2
	Quercus pubescens	1
pine	*Pinus sylvestris*	413
	Pinus nigra	125
	Pinus pinaster	19
	Pinus cembra	13
	Pinus mugo arborea	10
	Pinus nigra subsp. laricio	3
spruce	*Picea abies*	2073
	Picea sitchensis	10

2 Overview of forests plots in 2015

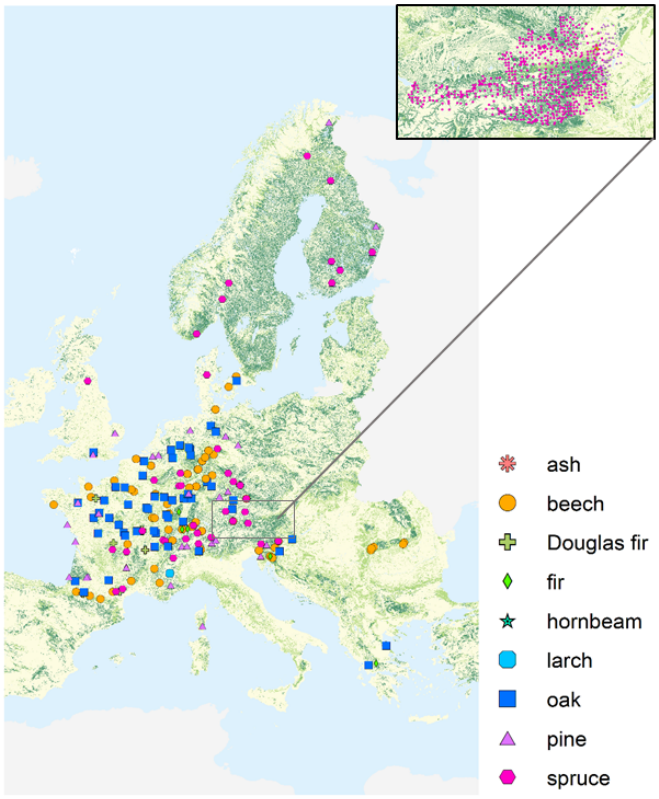

Figure S 1. Overview of forest plots, at which Hg foliage samples were harvested from different tree species groups during the sampling year 2015. The enlarged map view at the top right depicts sampling locations of the Bio-Indicator Grid in Austria. Use of base map authorized under European Commission reuse policy (EU, 2011).

3 Determination of the beginning of the growing season

3.1 Matching of observations from the PEP725 database to forest plots

We matched observations on the beginning of the growing season of coniferous tree species from the Pan European Phenological database PEP725 (Templ et al., 2018) to the corresponding closest forest plot of the respective sampling year (2015 or 2017) within our database. Complementing start-of-season modelling (Sect. 3.2) with conifer data from an external database was necessary, because the utilized PROBA-V LAI modelling method by Bórnez et al. (2020) (see Sect. 3.2) is validated with observations from deciduous tree species (beech, oak, birch, maple) only. Phenological observations of PEP725 sites are classified by BBCH (Biologische Bundesanstalt, Bundessortenamt and chemical industry) phenological scale. We used data for the beginning of the season for the following BBCH codes: 10, 11, 13, 31, 60, 61 and 223, which correspond to stages of leaf unfolding and first flowering. Matching was performed using the nearest neighbor function *matchpt* from the R Biobase package on coordinates of forest plots and PEP725 observation sites. We executed the nearest neighbor matching twice. In the first round, we gave latitude, longitude and altitude as input to the matching function. We exclusively matched latitude and altitude in a second round for forest plots with a difference between plot and PEP725 observation point larger than three degrees of latitude or 30 m of altitude (12% of plots). As a result, all distances between forest plots and PEP725 observation points are less than three degrees of latitude and 30 m of altitude, with an exception of around 6% of forest plots for which no such close PEP725 observation points were available. A lack of close PEP725 observation points was the case for forest plots in Norway (10 degrees of latitude), Greece (9 degrees of latitude), a few sites in Southern France/Corsica, Southern Switzerland and Austria, and one site in England and Romania respectively (3 – 6 degrees of latitude). Exceedances of 30 m of altitude difference between forest plots and PEP725 observations emerged for only 1% of sites with the maximum altitude difference being 350 m. As a result, the average beginning of the season DOY for conifers (86% spruce plots, 13% pine plots, 1% other conifers) is 127 $\pm$ 14 d which is one day earlier than the average start-of-season PEP725 observations for spruce from 1970 – 2009 (Basler, 2016).

3.2 PROBA-V LAI modelling of the beginning of the growing season

We utilized the leaf area index (LAI) product by Copernicus Global Land Service based on PROBA-V satellite imagery at a resolution of 300 m and 10 days (Fuster et al., 2020) to model the start of the growing season for deciduous trees as validated by Bórnez et al. (2020). This approach is part of the threshold based methods for growing season modelling (de Beurs and Henebry, 2010). Figure 2 gives an exemplary temporal sequence of PROBA-V LAIs from a forest plot in Switzerland. We defined the start of the growing season as the point in time when the LAI exceeds the 30% percentile of the amplitude between minimum LAI early in the year and maximum LAI at peak season. Bórnez et al. (2020) found, that a 30 % percentile amplitude threshold performs best (root mean squared error of 12.5 days; $R^2 = 0.62$) for PROBA-V LAI modelling when modelling results for the beginning of the growing season were compared to 359 ground phenological observations of deciduous tree species in Europe. In the present ICP Forests database there were three forest plots for which PROBA-V LAI modelling yielded unrealistic results, as the beginning of the growing season was either too early (forest plot Gontrode in 2017) or too late (forest plots Ehrhorn and Maron in 2015) in the season given their respective latitude and altitude. We replaced the beginning of the growing season DOY (day of year) at these three plots with 119 (April 29th) which equals the average beginning of the growing season DOY of deciduous tree species of the present dataset. Figure 3 presents an overview of the modelling results for beginning of the growing season DOYs at each deciduous forest plot per latitude. The coefficient of correlation of linear regression between beginning of growing season DOYs and latitude was positive and significant ($p < 0.01$), so as a tendency, the beginning of the growing season DOYs modelled here correspond to expected latitudinal differences. The average beginning of the growing season DOY (mean $\pm$ s.d. in days) is 120 $\pm$ 10 d for beech and 111 $\pm$ 11 d for oak. This average beginning of the growing season DOY for beech is consistent within an accuracy of 2 days with 7840 PEP725 observations from Central Europe between the years 1970 – 2009 (Basler, 2016). For oak, the modelled beginning of the growing season is 13 days earlier than the respective average DOY from 6400 PEP725 observations between 1970 – 2009 (Basler, 2016). This 13 d discrepancy could be due to the fact that the PEP725 oak beginning of season data evaluated by Basler (2016) comprise observations mainly from Germany, while 26% of oak samples in the current data set originated from more southern latitudes < 48°.

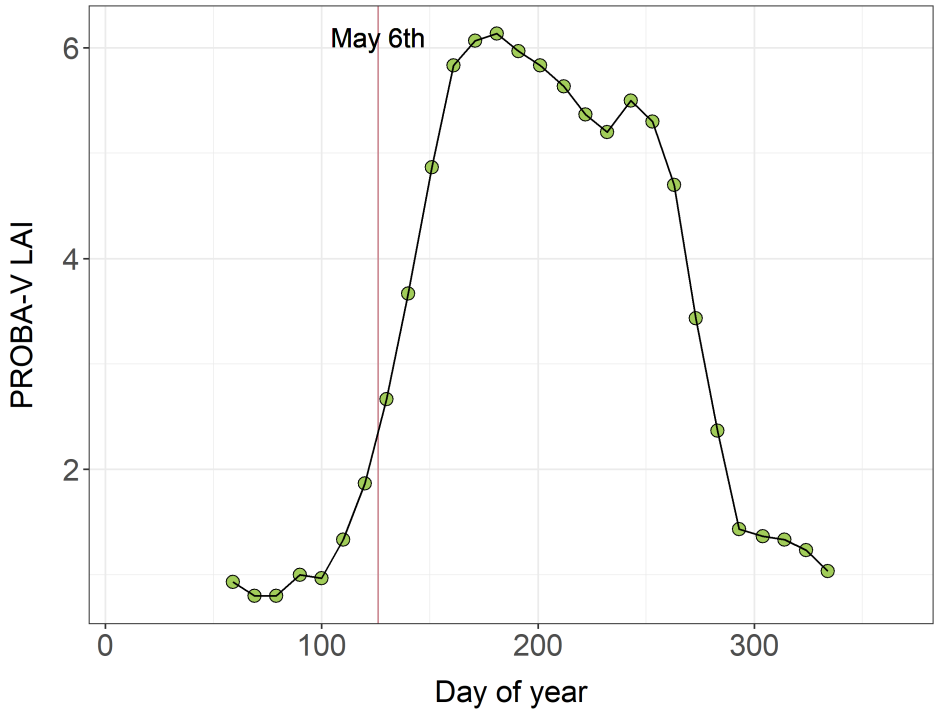

Figure S 2. Temporal development of the Copernicus LAI (leaf area index) values derived from PROBA-V satellite images (Fuster et al., 2020) at the Swiss forest research site Bettlachstock in 2017. The start-of-season is defined as the date, at which the LAI value exceeds the 30 percentile threshold of the amplitude between minimum LAI early in the year and maximum LAI at peak season following a modelling approach by Bórnez et al. (2020). Here the beginning of the growing season corresponds to May 6th 2017. This date is one week later than the average beginning of the growing season of this dataset for beech, which represents the main tree species at Bettlachstock. Given that Bettlachstock is located at 1101 m - 1196 m above sea level, however, May 6th is a plausible beginning of the growing season for beech at this site.

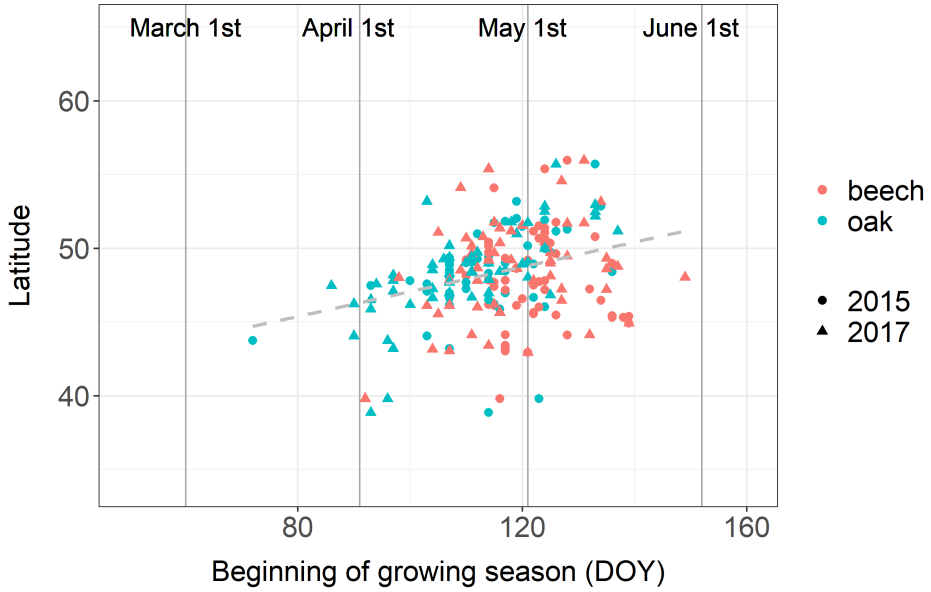

Figure S 3. Start-of-season DOY (day of year) at ICP Forests Level II plots resulting from growing season modelling approach after Bórnez et al. (2020)

3.3 Soil hydraulic parameters for modelling of stomatal closure

Table S 2. Soil texture specific soil water at field capacity (SW_{FC}) and at the permanent wilting point (SW_{PWP}), plant available water (PAW), and critical PAW (PAW_{crit}), below which plants were modelled to start to close their stomata. PAW equals the difference between SW_{FC} and SW_{PWP} and $PAW_{crit} = 0.5 \cdot PAW + WC_{PAW}$. All values are taken from Saxton and Rawls (2006) (Table 3) and represent units of $\mathbf{m}^3\ \mathbf{m}^{-3}$.

Soil texture	**SW_{FC}**	**SW_{PWP}**	**PAW**	**PAW_{crit}**
Sand	0.10	0.05	0.05	0.075
Loamy sand	0.12	0.05	0.07	0.085
Sandy loam	0.18	0.08	0.10	0.13
Sandy clay loam	0.27	0.17	0.10	0.22
Clay	0.42	0.30	0.12	0.36
Silty clay	0.41	0.27	0.14	0.34
Clay loam	0.36	0.22	0.14	0.29
Loam	0.28	0.14	0.14	0.21
Silty clay loam	0.38	0.22	0.16	0.30
Silt loam	0.31	0.11	0.20	0.21

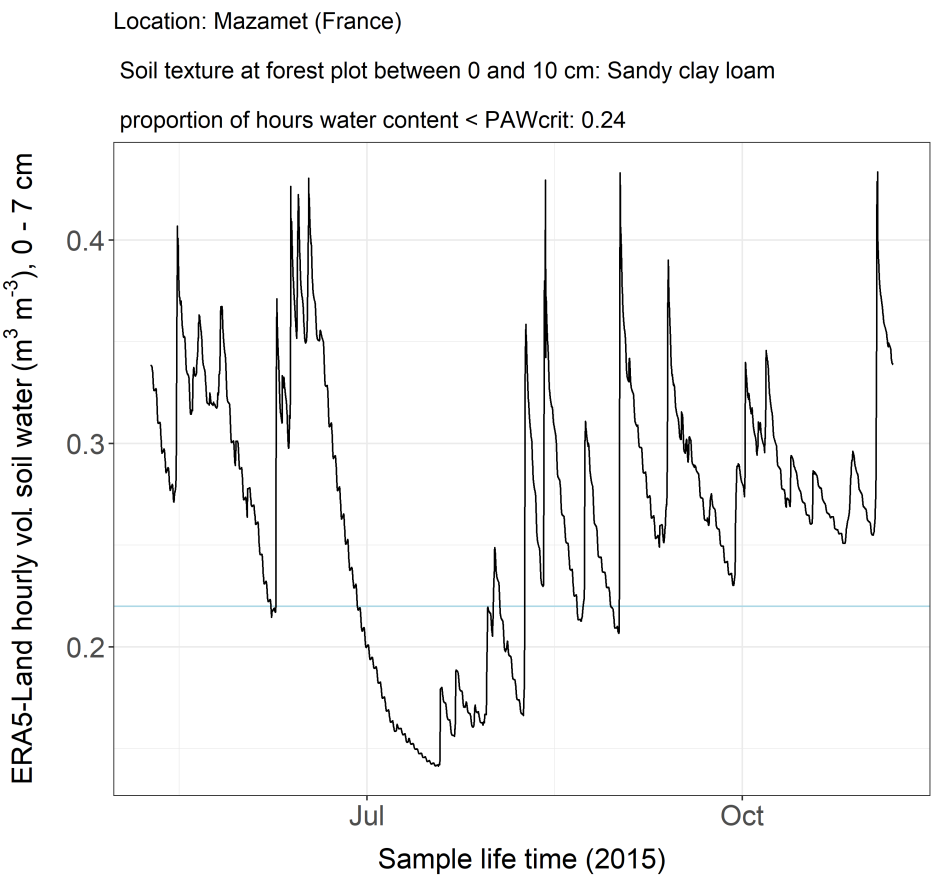

Figure S 4. Volumetric soil water (m^3 m^{-3}, layer 1) from the ERA5-Land hourly dataset (Muñoz Sabater, 2019) in the region of Mazamet (France) versus sample life period of the associated ICP Forests Level II Plot (plot code: 1-45). The lightblue line denotes the threshold value of plant available water (PAW_{crit}) of 0.22 m^3 m^{-3} for the soil texture (sandy clay loam) of this forest plot (compare Table 2, this document).

3.4 Calculation of median leaf stomatal conductance from data by Lin et al. (2015)

We calculated median stomatal conductance values from a global database of leaf-level gas exchange parameters compiled by Lin et al. (2015) from literature and unpublished sources. Stomatal conductance values from the following tree species were extracted from the database: beech (Fagus sylvatica), oak (Quercus petraea, Quercus robur), spruce (Picea abies) and pine (Pinus edulis, Pinus pinaster, Pinus sylvestris, Pinus taeda). All data were measured in Europe (Denmark, Finland, France, Germany, Sweden, UK) and North America. The following data contributors were named as data source for the data we used to calculate median stomatal conductance per tree species: Alexandre Bosc, D. Ellsworth, Jean-Marc Limousin, John Drake, Lasse Tarvainen, Maj-Lena Linderson, Mark Broadmeadow, Michael Freeman, Pasi Kolari, Reinhart Ceulemans and Mark Low. The database can be accessed at https://figshare.com/articles/dataset/Optimal_stomatal_behaviour_around_the_world/1304289.

3.5 Foliar Hg concentration over the growing season

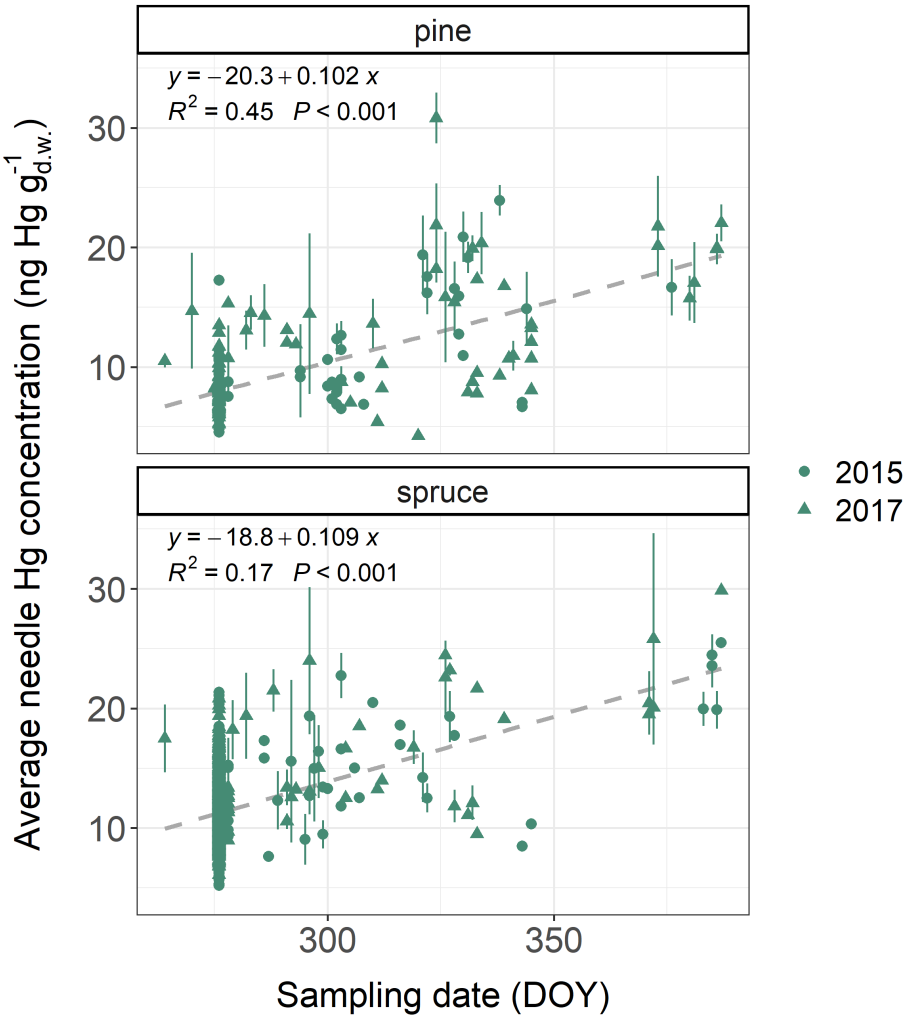

Figure S 5. Average foliar Hg concentrations (ng Hg $g_{d.w.}^{-1}$) per forest plot of pine and spruce samples versus respective sampling date (day-of-year of both 2015 and 2017). At some pine and spruce forest plots sampling took place in winter after 31st of December, such that day-of-year > 365. Error bars denote ± one standard deviation between multiple foliage samples at one forest plot. All samples represent current-season values.

4 Foliar Hg uptake per tree species

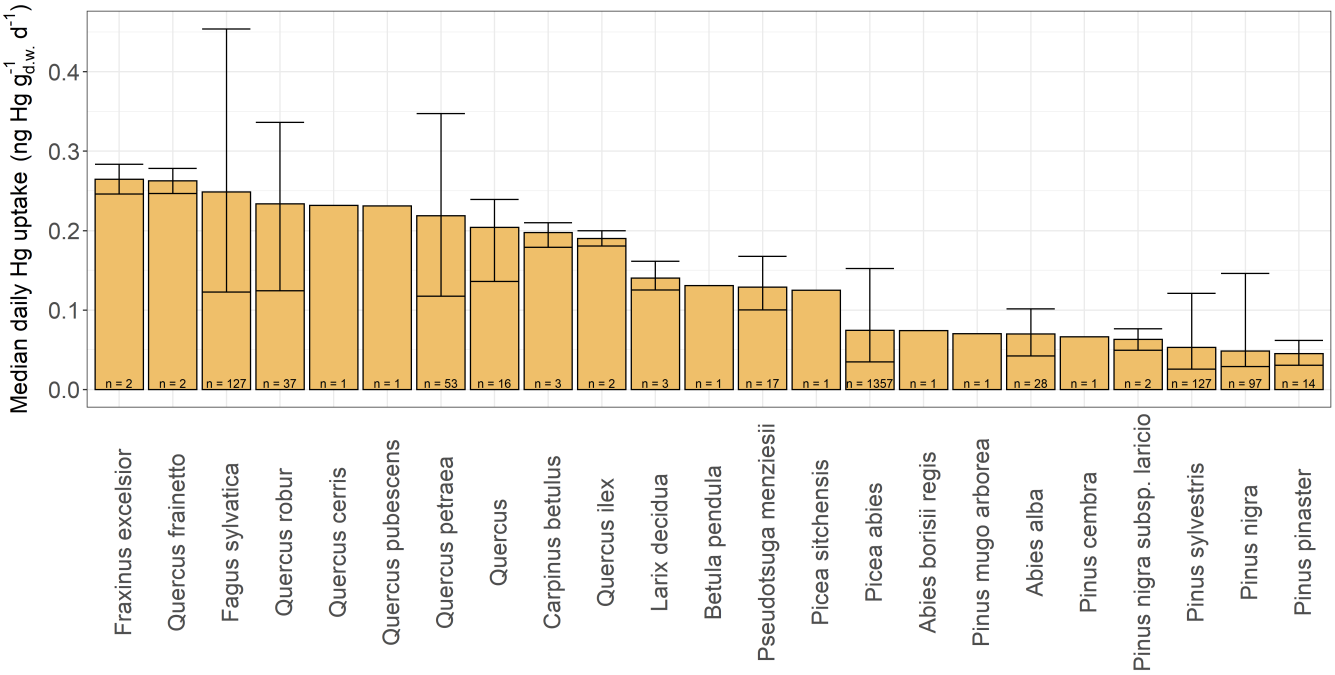

Figure S 6. Median daily foliar Hg uptake (ng Hg $g_{d.w.}^{-1}$ d^{-1}) of different tree species arranged from highest to lowest value. Error bars give the value range within each tree species and n indicates the number of sites at which the respective tree species were sampled in sum in the years 2015 and 2017. Foliar samples of evergreen coniferous tree species consist of needles of the current season. *Quercus* represents a mix of samples from *Quercus petraea* and *Quercus robur*.

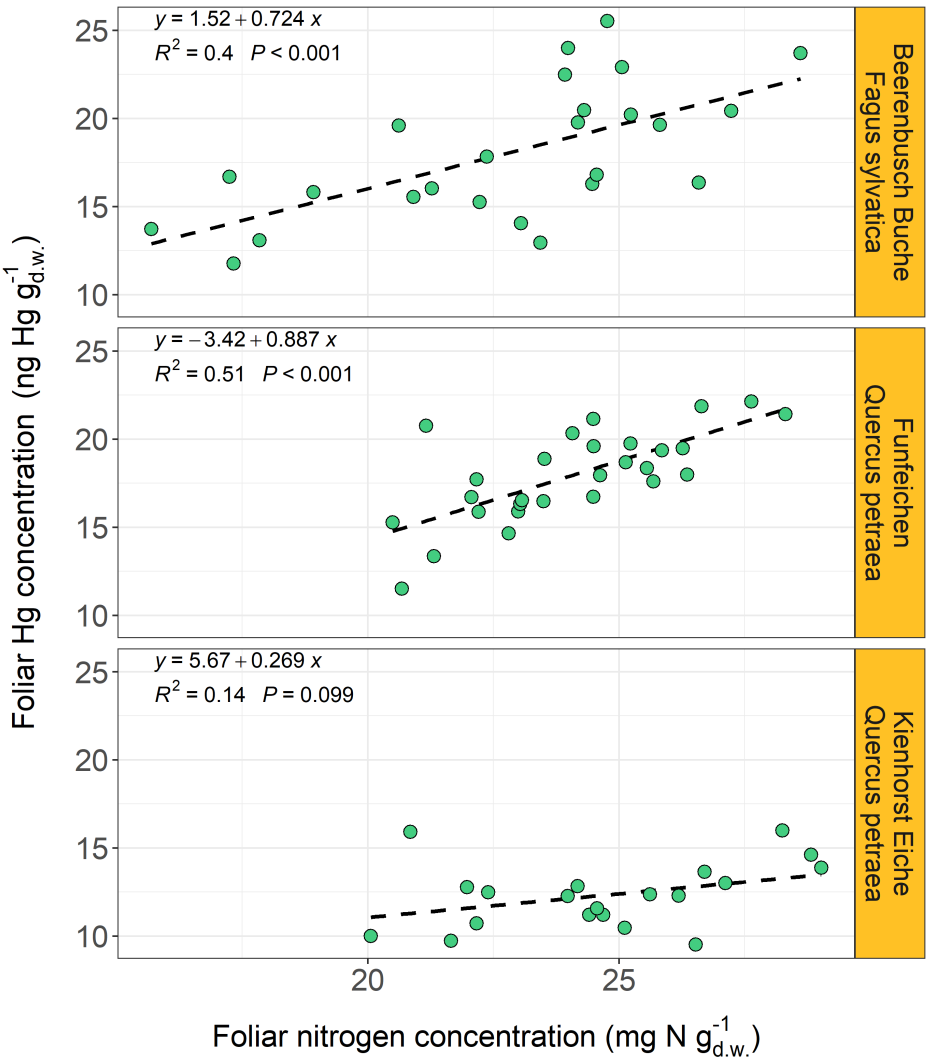

Figure S 7. Linear regression between foliar Hg concentrations (ng Hg $g_{d.w.}^{-1}$) and leaf nitrogen concentration (mg N $g_{d.w.}^{-1}$) exemplary for one beech (Fagus sylvatica, top) and two oak (Quercus petraea) forest plots in Brandenburg, Germany.

6 Foliar Hg uptake and proportion of VPD threshold hours

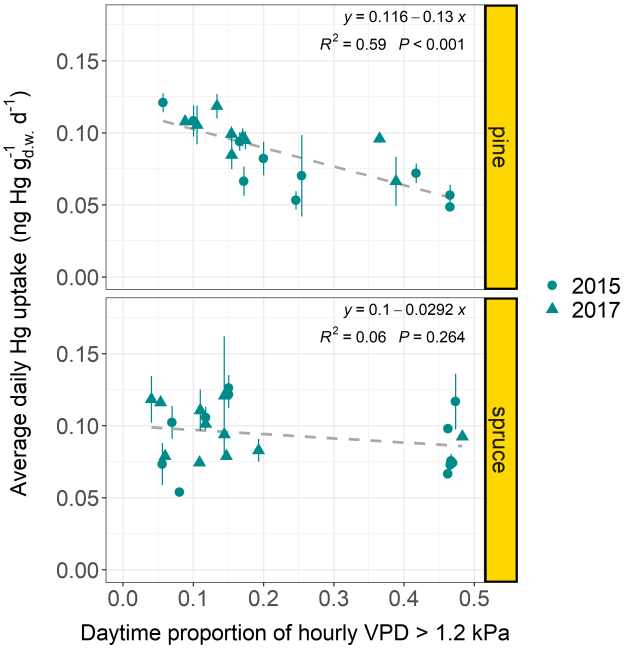

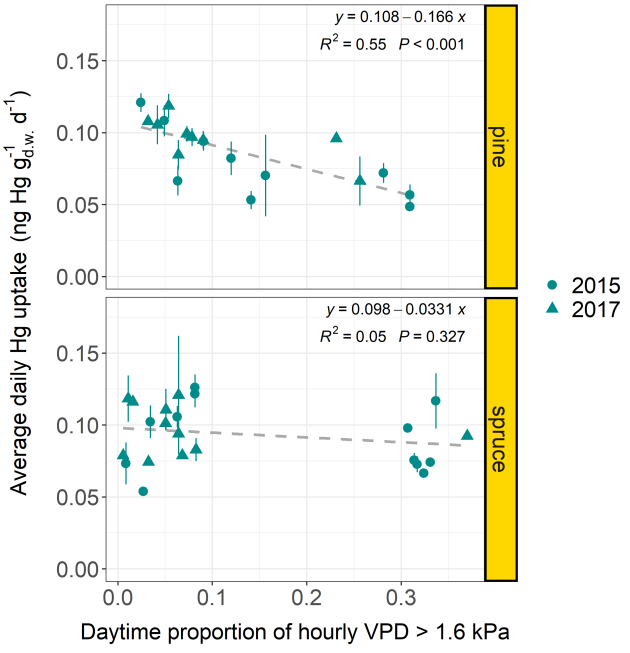

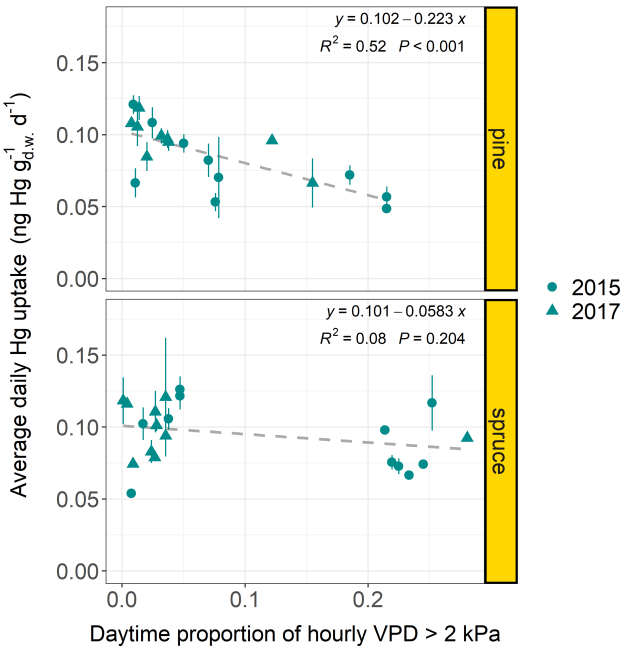

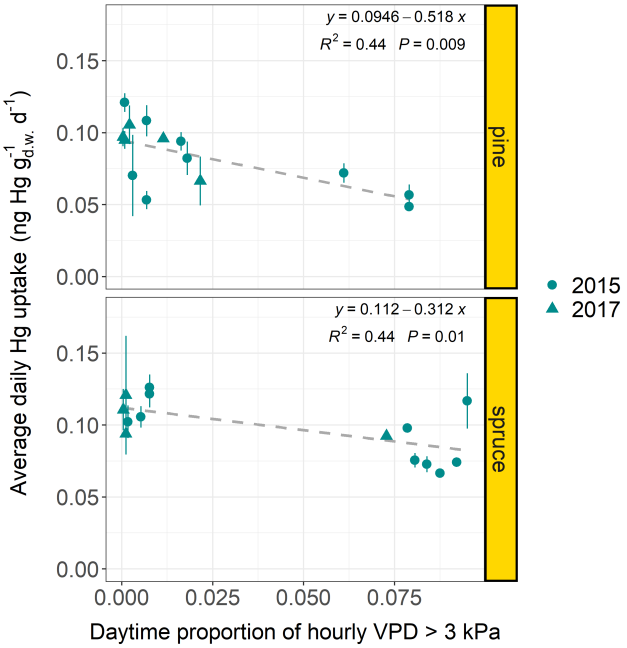

Figure S 8. Average daily foliar Hg uptake rates (ng Hg $g_{d.w.}^{-1}$ d^{-1}) of current-season pine and spruce needles per forest plot sampled in 2015 and 2017 versus the proportion of hours within an average day of the respective sample life periods, during which the average hourly daytime (06:00 - 18:00 LT) vapor pressure deficit (VPD) exceeded a threshold value of 1.2 kPa, 1.6 kPa, 2 kPa and 3 kPa respectively. Error bars denote ± one standard deviation between multiple samples at each forest plot.

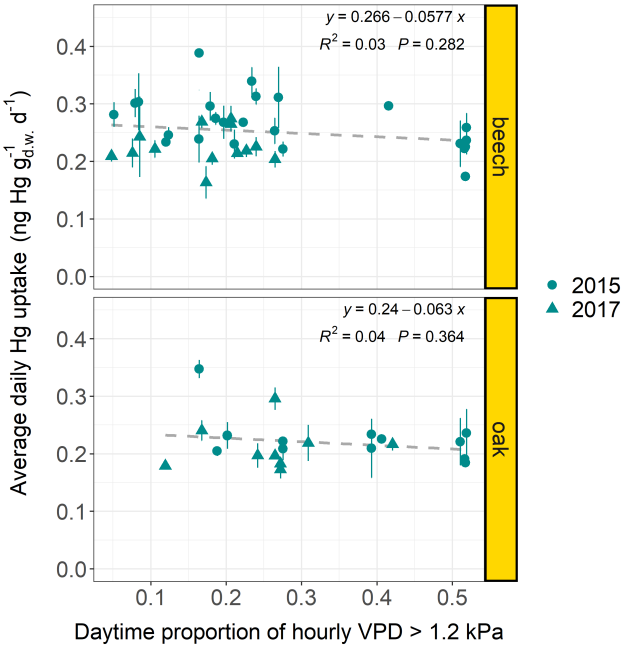
y = 0.266 − 0.0577 x
R² = 0.03 P = 0.282
beech
y = 0.24 − 0.063 x
R² = 0.04 P = 0.364
oak
2015
2017
Average daily Hg uptake (ng Hg g⁻¹d.w. d⁻¹)
Daytime proportion of hourly VPD > 1.2 kPa

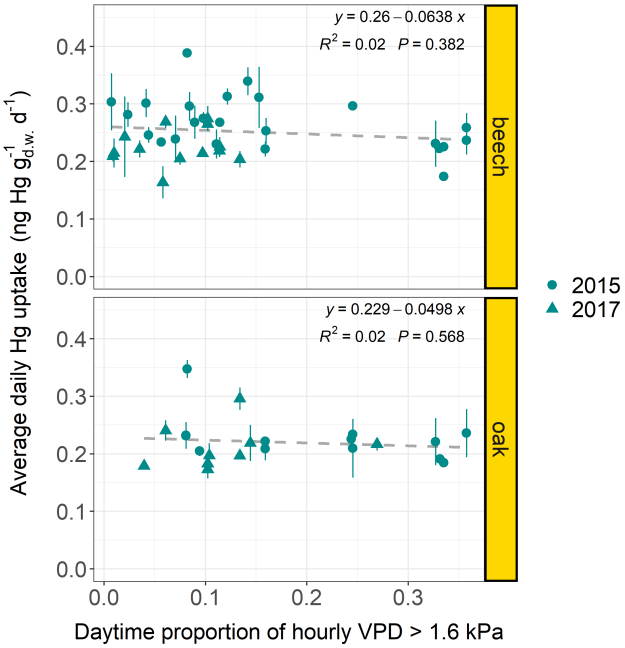
y = 0.26 − 0.0638 x
R² = 0.02 P = 0.382
beech
y = 0.229 − 0.0498 x
R² = 0.02 P = 0.568
oak
2015
2017
Average daily Hg uptake (ng Hg g⁻¹d.w. d⁻¹)
Daytime proportion of hourly VPD > 1.6 kPa

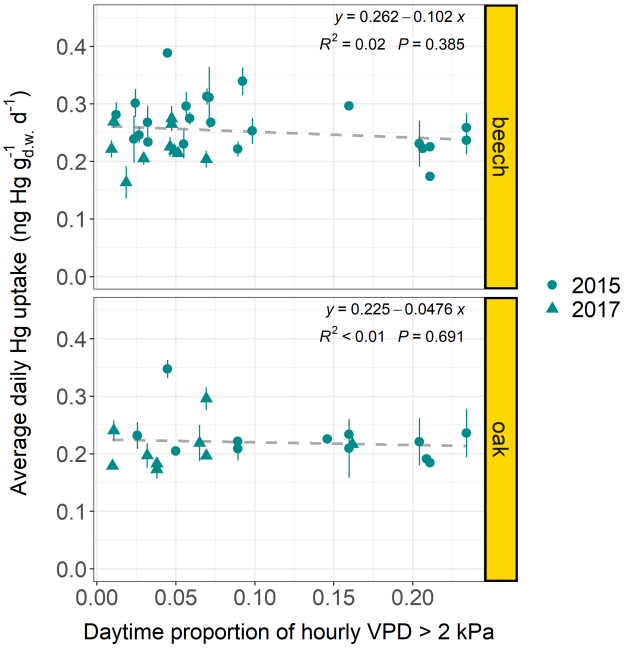

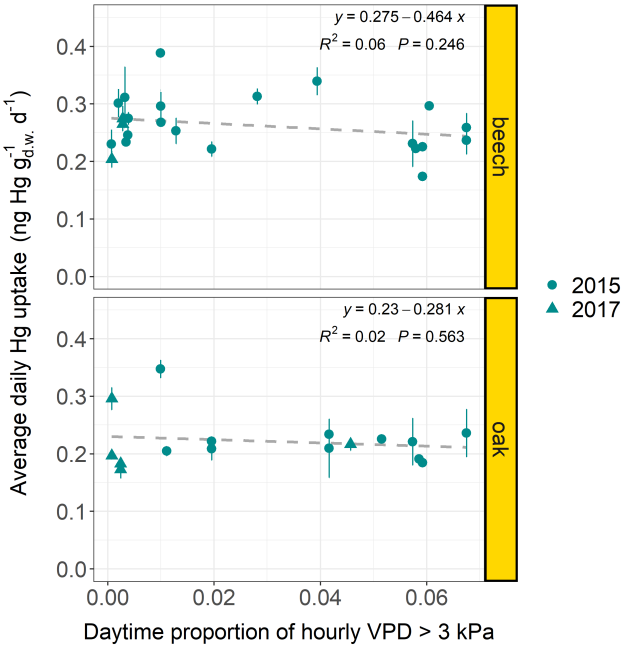

Figure S 9. Average daily foliar Hg uptake rates (ng Hg $g_{d.w.}^{-1}$ d^{-1}) of beech and oak leaves per forest plot sampled in 2015 and 2017 versus the proportion of hours within an average day of the respective sample life periods, during which the average hourly daytime (06:00 - 18:00 LT) vapor pressure deficit (VPD) exceeded a threshold value of 1.2 kPa, 1.6 kPa, 2 kPa and 3 kPa respectively. Error bars denote ± one standard deviation between multiple samples at each forest plot.

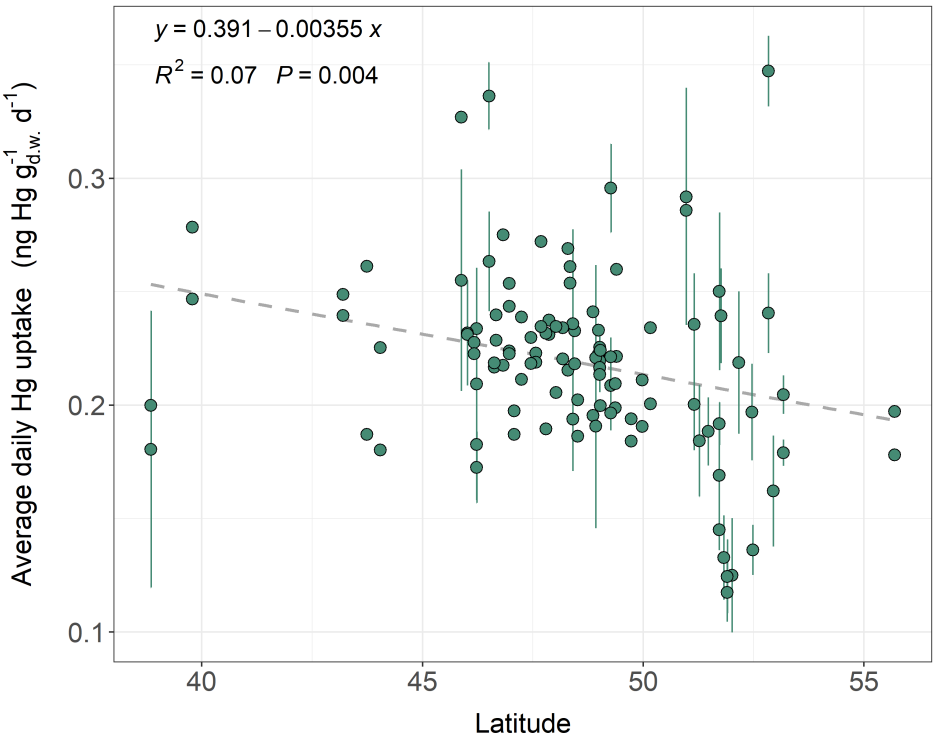

Figure S 10. Linear regression of average **oak** leaf Hg uptake rates (ng Hg $g_{d.w.}^{-1}$ d^{-1}) per forest plot versus latitude. Where available, error bars denote ± one standard deviation of multiple oak trees at one forest plot.

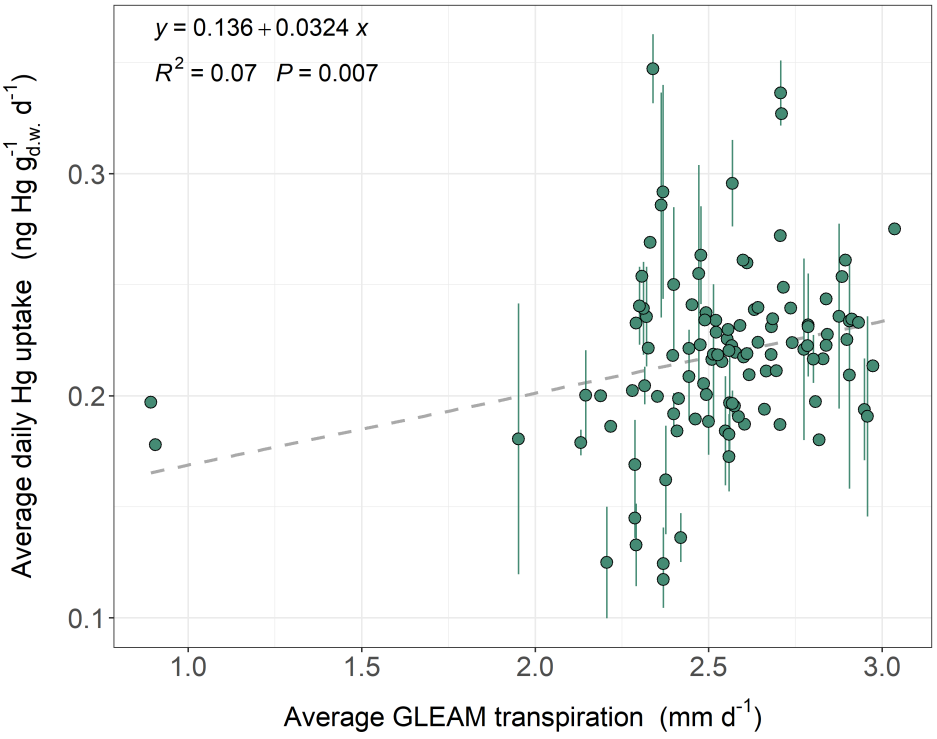

Figure S 11. Linear regression of average **oak** leaf Hg uptake rates (ng Hg $g_{d.w.}^{-1}$ d^{-1}) per forest plot versus average GLEAM transpiration (mm d^{-1}). Where available, error bars denote $\pm$ one standard deviation of multiple oak trees at one forest plot.

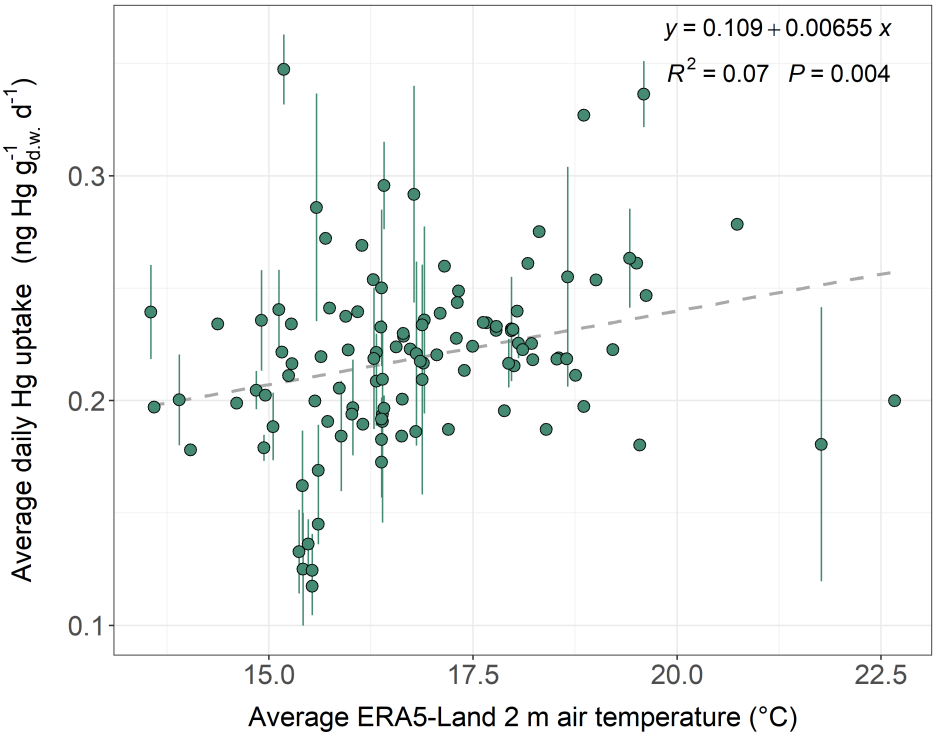

Figure S 12. Linear regression of average **oak** leaf Hg uptake rates (ng Hg $g_{d.w.}^{-1}$ d^{-1}) per forest plot versus average ERA5-Land hourly 2 m air temperatures (°C) during the respective sample life periods. Where available, error bars denote ± one standard deviation of multiple oak trees at one forest plot.

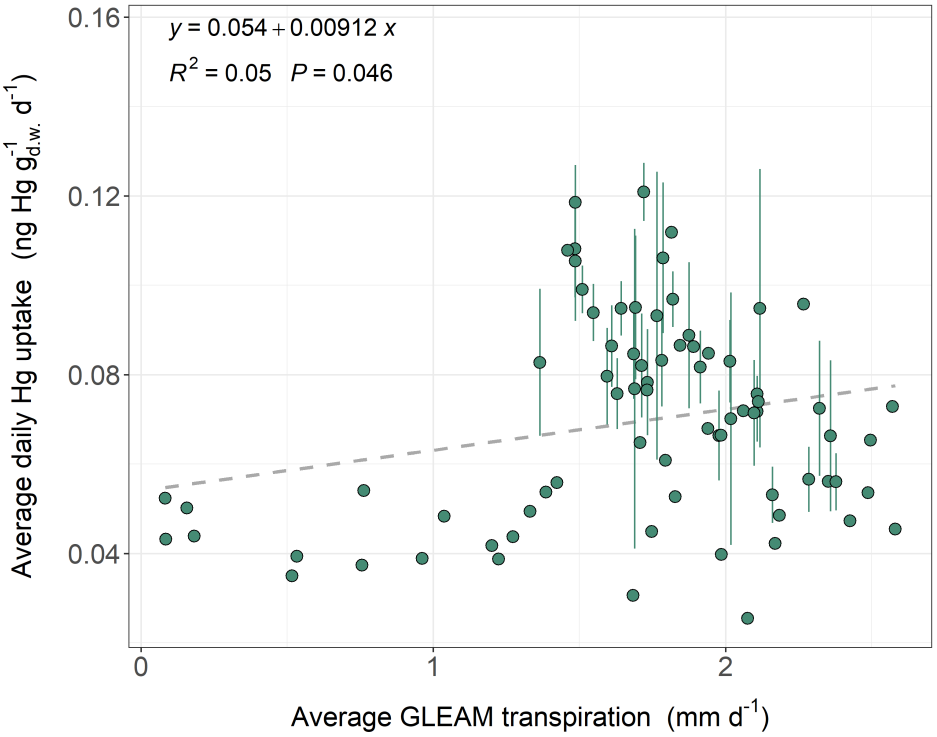

Figure S 13. Linear regression of average **pine** needle Hg uptake rates (ng Hg $g_{d.w.}^{-1}$ d^{-1}) per forest plot versus average GLEAM transpiration (mm d^{-1}). Where available, error bars denote $\pm$ one standard deviation of multiple pine trees at one forest plot. All needle values represent the current-season.

Table S 3. Species-specific daily foliar Hg uptake (mean ± sd; ng Hg $g_{d.w.}^{-1}$ d^{-1}; rounded to two decimals) resolved for the sampling years 2015 and 2017 and difference between respective average daily foliar Hg uptake rates of 2015 - average daily foliar Hg uptake rates of 2017.

Species group	sampling year	Daily Hg uptake (mean ± sd) (ng Hg $g_{d.w.}^{-1}$ d^{-1})	Diff. daily Hg uptake (2015 - 2017)	n sites
beech	2015	0.27 ± 0.05	0.04	51
	2017	0.23 ± 0.04		
Douglas fir	2015	0.12 ± 0.02	- 0.02	7
	2017	0.14 ± 0.02		
fir	2015	0.07 ± 0.02	- 0.005	6
	2017	0.08 ± 0.02		
oak	2015	0.23 ± 0.04	0.004	49
	2017	0.22 ± 0.03		
pine	2015	0.05 ± 0.02	∼ 0	107
	2017	0.05 ± 0.02		
spruce	2015	0.07 ± 0.02	- 0.003	658
	2017	0.08 ± 0.02		

References

Basler, D.: Evaluating phenological models for the prediction of leaf-out dates in six temperate tree species across central Europe, 217, 10–21, https://doi.org/10.1016/j.agrformet.2015.11.007, 2016.

Bórnez, K., Descals, A., Verger, A., and Peñuelas, J.: Land surface phenology from VEGETATION and PROBA-V data. Assessment over deciduous forests, 84, 101 974, https://doi.org/10.1016/j.jag.2019.101974, 2020.

de Beurs, K. M. and Henebry, G. M.: Spatio-Temporal Statistical Methods for Modelling Land Surface Phenology, in: Phenological Research: Methods for Environmental and Climate Change Analysis, edited by Hudson, I. L. and Keatley, M. R., pp. 177–208, Springer Netherlands, https://doi.org/10.1007/978-90-481-3335-2_9, 2010.

EU: European Commission, 2011/833/EU: Commission Decision of 12 December 2011 on the reuse of Commission documents, https://eur-lex.europa.eu/eli/dec/2011/833/oj, 2011.

Fuster, B., Sánchez-Zapero, J., Camacho, F., García-Santos, V., Verger, A., Lacaze, R., Weiss, M., Baret, F., and Smets, B.: Quality Assessment of PROBA-V LAI, fAPAR and fCOVER Collection 300 m Products of Copernicus Global Land Service, 12, 1017, https://doi.org/10.3390/rs12061017, number: 6 Publisher: Multidisciplinary Digital Publishing Institute, 2020.

Lin, Y.-S., Medlyn, B. E., Duursma, R. A., Prentice, I. C., Wang, H., Baig, S., Eamus, D., de Dios, V. R., Mitchell, P., Ellsworth, D. S., de Beeck, M. O., Wallin, G., Uddling, J., Tarvainen, L., Linderson, M.-L., Cernusak, L. A., Nippert, J. B., Ocheltree, T. W., Tissue, D. T., Martin-StPaul, N. K., Rogers, A., Warren, J. M., De Angelis, P., Hikosaka, K., Han, Q., Onoda, Y., Gimeno, T. E., Barton, C. V. M., Bennie, J., Bonal, D., Bosc, A., Löw, M., Macinins-Ng, C., Rey, A., Rowland, L., Setterfield, S. A., Tausz-Posch, S., Zaragoza-Castells, J., Broadmeadow, M. S. J., Drake, J. E., Freeman, M., Ghannoum, O., Hutley, L. B., Kelly, J. W., Kikuzawa, K., Kolari, P., Koyama, K., Limousin, J.-M., Meir, P., Lola da Costa, A. C., Mikkelsen, T. N., Salinas, N., Sun, W., and Wingate, L.: Optimal stomatal behaviour around the world, 5, 459–464, https://doi.org/10.1038/nclimate2550, number: 5 Publisher: Nature Publishing Group, 2015.

Muñoz Sabater, J.: ERA5-Land hourly data from 1981 to present. Copernicus Climate Change Service (C3S) Climate Data Store (CDS), https://doi.org/https://cds.climate.copernicus.eu/cdsapp#!/dataset/reanalysis-era5-land?tab=overview, 2019.

Saxton, K. E. and Rawls, W. J.: Soil Water Characteristic Estimates by Texture and Organic Matter for Hydrologic Solutions, 70, 1569–1578, https://doi.org/10.2136/sssaj2005.0117, _eprint: https://acsess.onlinelibrary.wiley.com/doi/pdf/10.2136/sssaj2005.0117, 2006.

Templ, B., Koch, E., Bolmgren, K., Ungersböck, M., Paul, A., Scheifinger, H., Rutishauser, T., Busto, M., Chmielewski, F.-M., Hájková, L., Hodzić, S., Kaspar, F., Pietragalla, B., Romero-Fresneda, R., Tolvanen, A., Vučetič, V., Zimmermann, K., and Zust, A.: Pan European Phenological database (PEP725): a single point of access for European data, 62, 1109–1113, https://doi.org/10.1007/s00484-018-1512-8, 2018.